JOURNAL OF MATERIALS SCIENCE 21 (1986) 1441–1447

Directionally solidified Bi_2O_3–$6Bi_2O_3 \cdot SiO_2$ eutectic

T. KOKUBO, H. KIM
Institute for Chemical Research, Kyoto University, Uji, Kyoto-Fu 611, Japan

The phase diagrams of the systems Bi_2O_3–$6Bi_2O_3 \cdot SiO_2$ and $(Bi_2O_3)_{0.85}$ $(Nb_2O_5)_{0.15}$–$6Bi_2O_3 \cdot SiO_2$ were determined by a quenching method. Melts of the eutectic and neighbouring compositions in these systems were unidirectionally solidified at various rates of 0.5 to 10 mm h^{-1} under a temperature gradient of 100° C cm^{-1}. At any solidification rate examined, the ingot was of irregular structure in the former system and was of well-aligned regular structure in the latter system at the eutectic composition and those deviated from that by 10 mol%. In the latter ingots, fibrous δ-$(Bi_2O_3)_{0.85}$ $(Nb_2O_5)_{0.15}$ crystals were embedded in parallel and with a uniform spacing in a matrix of γ-$6Bi_2O_3 \cdot SiO_2$ crystal. The diameter, d, of the fibrous crystals and the interfibre spacing λ decreased from 3.8 to 0.7 μm and 10 to 1.9 μm, respectively, with increasing solidification rate, R, in the range 0.5 to 10 mm h^{-1}, following the relations $d = 2.5R^{-1/2}$ and $\lambda = 6.9R^{-1/2}$. The volume fraction of the fibrous crystals increased from 0.14 to 0.23 with an increase in the $(Bi_2O_3)_{0.85}$ $(Nb_2O_5)_{0.15}$ content of the melt from 46 to 66 mol%. The elongation direction $\langle 1\,1\,0 \rangle$ of the fibrous crystal was parallel to the $\langle 1\,1\,1 \rangle$ direction of the matrix crystal. The difference in the microstructure of the ingots between the systems is discussed in terms of the solidification process.

1. Introduction

γ-$6Bi_2O_3 \cdot SiO_2$ crystal is a useful material for optical applications such as image storage devices [1, 2], since it is photoconductive [3], electrooptic [3], optically active [3] and photorefractive [4]. The authors previously revealed that large transparent polycrystalline [5] and single-crystal [6] plates of this phase are fairly easily obtained by a unidirectional solidification of melt using a temperature gradient furnace.

Composites of the γ-$6Bi_2O_3 \cdot SiO_2$ with other crystals, having a well-aligned microstructure, might be also useful for various optical applications as image detector and display systems with a high resolution. In the present study, we attempted to prepare such composites by a unidirectional solidification of melts of the eutectic and neighbouring compositions in the systems Bi_2O_3–$6Bi_2O_3 \cdot SiO_2$ and $(Bi_2O_3)_{0.85}$ $(Nb_2O_5)_{0.15}$–$6Bi_2O_3 \cdot SiO_2$.

2. Experimental details

2.1. Determination of the phase diagram

A phase diagram of the system Bi_2O_3–$6Bi_2O_3 \cdot SiO_2$ (B–BS) was previously reported by Levin and Roth [7]. The eutectic point is, however, not precisely determined. No phase diagram was reported of the system $(Bi_2O_3)_{0.85}$ $(Nb_2O_5)_{0.15}$–$6Bi_2O_3 \cdot SiO_2$ (BN–BS).

About 10 g powder mixtures of various compositions comprised of reagent grade chemicals of Bi_2O_3, SiO_2 and Nb_2O_5 (purities > 99.9%) were calcined at 750° C in the former system and 850° C in the latter system both for 10 h, cooled and then pulverized into grains of −200 mesh (74 μm opening). A part of the powder was subjected to differential thermal analysis with a heating rate of 10° C min^{-1}, in order to determine approximate solidus and liquidus temperatures.

Another portion of powder was put into a small platinum cone, which was attached to the tip of a thermocouple, and placed in a platinum furnace, the temperature of which was kept at a given temperature, for 30 min. After heating, the powder was quenched into water and examined under a polarizing microscope as to whether it had been melted or not.

2.2. Unidirectional solidification of the melt

Approximately 250 g powder mixture for the various compositions in the systems B–BS and BN–BS were prepared from the reagent grade chemicals. The mixture was put into a 50 ml platinum crucible of 60 mm diameter at the top, 30 mm diameter at the bottom and 35 mm deep, tightly covered with a platinum lid and calcined at 750° C in the system B–BS, and 850° C in the system BN–BS, both for 10 h.

The crucible containing the calcined material was placed on a water-cooled copper jacket in a SiC furnace shown in Fig. 1. The temperature at the top of the crucible was raised up to 1100 and 1180° C, respectively, for the B–BS and BN–BS systems so that the calcined material could be melted except for a thin layer 1 to 2 mm thick near the bottom. After being kept there for 5 h, the temperature at the top of the crucible was lowered at various rates from 5 to 100° C h^{-1} so that the melt was unidirectionally solidified at various rates from 0.5 to 10 mm h^{-1} under a temperature gradient of 100° C cm^{-1}. The calcined materials near the bottom which were not melted acted as seed crystals.

0022–2461/86 $03.00 + .12

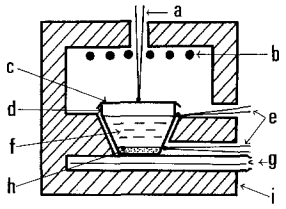

Figure 1 Temperature gradient furnace used for unidirectional solidification: a and e, thermocouple; b, SiC heating elements; c, platinum lid; d, platinum crucible; f, melt; g, water-cooled copper jacket; h, calcined raw materials; i, refractory.

The temperature gradient was calculated by dividing the temperature difference between the upper surface of the melt and the non-melted calcined material by the distance between them, before solidification. This temperature gradient was assumed to be maintained during the solidification. The solidification rate was calculated by dividing the cooling rate at the top of the crucible by the temperature gradient described above. In this calculation, the melt was assumed to be cooled at the same rate as that at the top of the crucible at any depth. These assumptions had been previously confirmed to be valid [5].

The solidified ingot was removed from the crucible by tapping the outside of the crucible with a plastic hammer.

2.3. Analysis of microstructure

2.3.1. X-ray diffraction

Crystalline phases precipitated in the solidified ingots were identified by powder X-ray diffraction. The Nb_2O_5 content of the precipitated δ-Bi_2O_3 crystal was determined by comparing its lattice constant with those of the δ-Bi_2O_3 crystals containing the known amounts of Nb_2O_5. The reference crystals were prepared by heating powder mixtures of Bi_2O_3 and Nb_2O_5 in various ratios at 850° C for 10 h.

Crystallographic orientation of the precipitated crystals were determined by X-ray diffraction of plate specimens which had been transversely and longitudinally cut from the ingots.

2.3.2. Optical microscopic observation

Microstructures of the ingots were observed for the transverse and longitudinal sections under metallurgical and polarizing microscopes. The diameter of the fibrous crystals was determined on the transverse sections. The interfibre spacing, λ, and the volume fraction, V, of the fibrous crystals were determined from the diameter, d, and the number, N, of the fibrous crystals observed in the area, S, on the transverse sections by using the relations

$$\lambda = \frac{(2S)^{1/2}}{3^{1/4} N^{1/2}} \quad (1)$$

$$V = \frac{\pi d^2 N}{4S} \quad (2)$$

3. Results

3.1. Phase diagram

The phase diagram near the eutectic points, which were determined by the quenching method, are shown in Figs. 2 and 3 for the systems Bi_2O_3–$6Bi_2O_3 \cdot SiO_2$ and $(Bi_2O_3)_{0.85}$ $(Nb_2O_5)_{0.15}$–$6Bi_2O_3 \cdot SiO_2$, respectively. It can be seen from these figures that the eutectic point is located at 98.3 (Bi_2O_3) · 1.7 $(6Bi_2O_3 \cdot SiO_2)$ in mol % and at 805° C in the system B–BS, and at 56.2 $(Bi_2O_3)_{0.85}$ $(Nb_2O_5)_{0.15}$ · 43.8 $(6Bi_2O_3 \cdot SiO_2)$ in mol % and at 894° C in the system BN–BS.

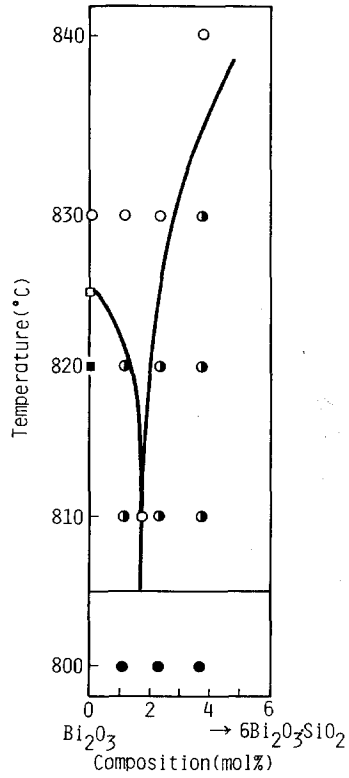

Figure 2 Phase diagram of the system Bi_2O_3–$6Bi_2O_3 \cdot SiO_2$: ○, liquid; ◑, liquid + crystal (δ-Bi_2O_3 or γ-$6Bi_2O_3 \cdot SiO_2$); ●, crystal (δ-Bi_2O_3 + γ-$6Bi_2O_3 \cdot SiO_2$); ■, crystal (δ-Bi_2O_3); □, melting point reported by Levin and Roth [7].

3.2. Microstructure

3.2.1. B–BS system

Fig. 4 shows optical micrographs of transverse and longitudinal sections of the ingot of the eutectic composition in the system B–BS, which was solidified at a rate of 0.5 mm h^{-1}. Other solidification rates gave similar structures. Fig. 5 shows optical micrographs of transverse and longitudinal sections of the ingots of the compositions which deviated from the eutectic composition by 0.5 mol % toward each of the Bi_2O_3 and $6Bi_2O_3 \cdot SiO_2$, i.e. 98.8 (Bi_2O_3) · 1.2 $(6Bi_2O_3 \cdot SiO_2)$ and 97.8 (Bi_2O_3) · 2.2 $(6Bi_2O_3 \cdot SiO_2)$ in mol %, which were solidified at a rate of 0.5 mm h^{-1}.

Figs. 4 and 5 show that a well-aligned regular structure typical for eutectics cannot be obtained in the system B–BS even at the lowest solidification rate examined. The dispersed and the matrix phases were identified as γ-$6Bi_2O_3 \cdot SiO_2$ and α-Bi_2O_3 crystals, respectively, by optical microscopic observation and powder X-ray diffraction, as expected from the phase diagram. The δ-Bi_2O_3 phase transforms into the α-Bi_2O_3 phase below 730° C [7].

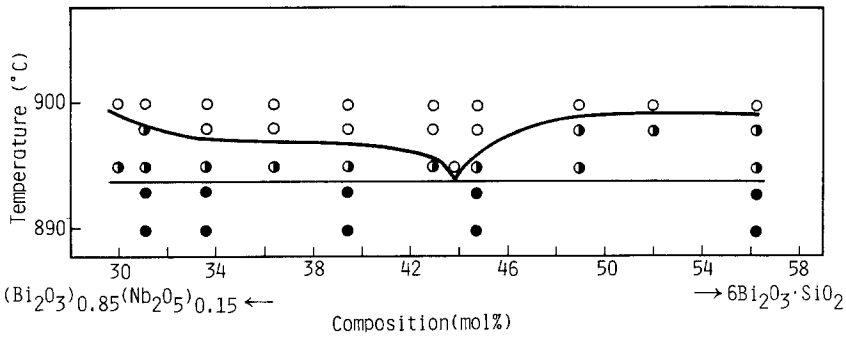

Figure 3 Phase diagram of the system $(Bi_2O_3)_{0.85}$ $(Nb_2O_5)_{0.15}$–$6Bi_2O_3 \cdot SiO_2$: ○, liquid; ◑, liquid + crystal (δ-Bi_2O_3 (Nb_2O_5) or γ-$6Bi_2O_3 \cdot SiO_2$); ●, crystal (δ-Bi_2O_3 (Nb_2O_5) + γ-$6Bi_2O_3 \cdot SiO_2$).

3.2.2. BN–BS system

Fig. 6 shows optical micrographs of transverse and longitudinal sections of the ingot of the eutectic composition in the system BN–BS, which was solidified at a rate of 0.5 mm h^{-1}. Parts of the left-hand side pictures were enlarged and are shown on the right-hand side.

Fig. 6 shows that a well-aligned fibrous regular structure (c and d) is obtained at this composition, although the structure is not uniform throughout the ingot but consisted of a number of regions (a and b) with crystal alignment a little different from region to region. The fibrous and the matrix phases were identified as δ-Bi_2O_3 (Nb_2O_5) and γ-$6Bi_2O_3 \cdot SiO_2$ crystals, respectively, by optical microscopic observation and powder X-ray diffraction, as expected from the phase diagram. The Nb_2O_5 content of the δ-Bi_2O_3 (Nb_2O_5) crystal determined from the lattice constant was 0.15 in mol fraction. The X-ray diffraction of a transverse section showed that the elongation direction of the fibrous δ-Bi_2O_3 (Nb_2O_5) crystal crystallographically corresponds to its ⟨1 1 0⟩ direction and this direction is parallel to the ⟨1 1 1⟩ direction of the matrix γ-$6Bi_2O_3 \cdot SiO_2$ crystal. These directions were exactly perpendicular to the bottom of the crucible in some regions, but a little tilted in other regions. The volume fraction of the fibrous crystals determined by the Equation 2 was 0.17.

Fig. 7 shows optical micrographs of transverse sections of the ingots of the eutectic composition in the system BN–BS, which were solidified at a rate of 1.0, 2.5, 5.0 and 10 mm h^{-1}, in comparison with that of the ingot solidified at a rate of 0.5 mm h^{-1}. It can be seen from Fig. 7 that the well-aligned regular structure is obtained also at a solidification rate as high as 10 mm h^{-1} at this eutectic composition. The diameter of the fibrous crystals and the interfibre spacing decreased from 3.8 to 0.7 μm and 10 to 1.9 μm, respectively, with increasing solidification rate in the range from 0.5 to 10 mm h^{-1}. The volume fractions of the fibrous crystals were 0.17 for all the solidification rates.

Fig. 8 shows optical micrographs of transverse sections which were cut from the upper part of the ingots of the compositions which deviated from the eutectic composition by 10 mol % toward each of the $(Bi_2O_3)_{0.85}(Nb_2O_5)_{0.15}$ and $6Bi_2O_3 \cdot SiO_2$, i.e. 66.2 $(Bi_2O_3)_{0.85}$ $(Nb_2O_5)_{0.15}$ · 33.8 $(6Bi_2O_3 \cdot SiO_2)$ and 46.2 $(Bi_2O_3)_{0.85}$ $(Nb_2O_5)_{0.15}$ · 53.8 $(6Bi_2O_3 \cdot SiO_2)$ in mol %. The solidification rate was 0.5 mm h^{-1} for both compositions. It can be seen from Fig. 8 that the well-aligned regular structure is also obtained at the compositions which deviated far from the eutectic compositions in the system BN–BS. The volume fractions of the fibrous crystals were 0.23 and 0.14 for the respective composition. The diameters of the fibrous

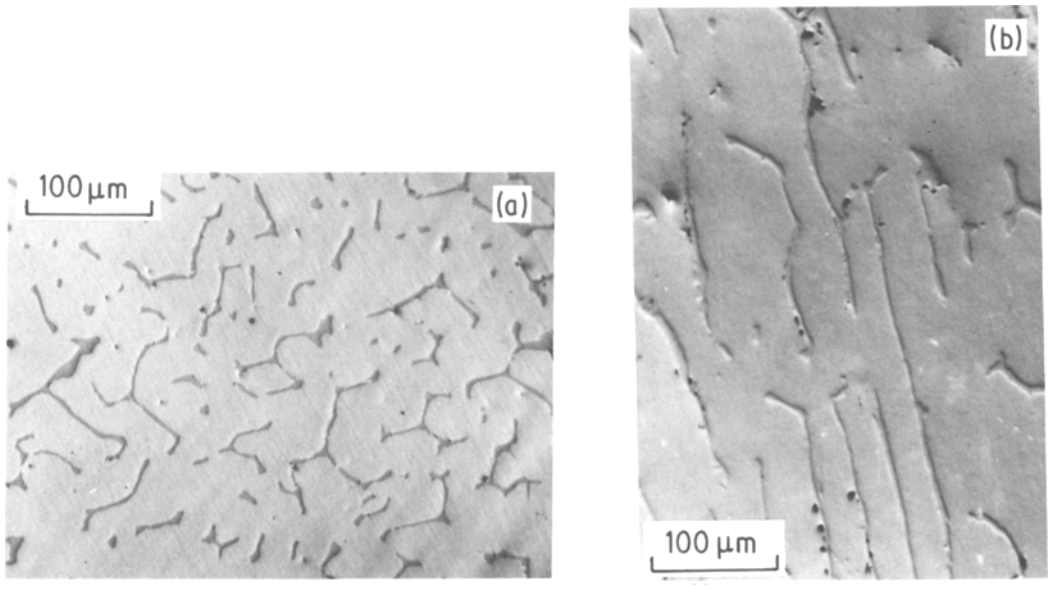

Figure 4 Metallurgical micrographs of transverse (a) and longitudinal (b) sections of the ingot of the eutectic composition in the system B–BS, which was solidified at a rate of 0.5 mm h^{-1}.

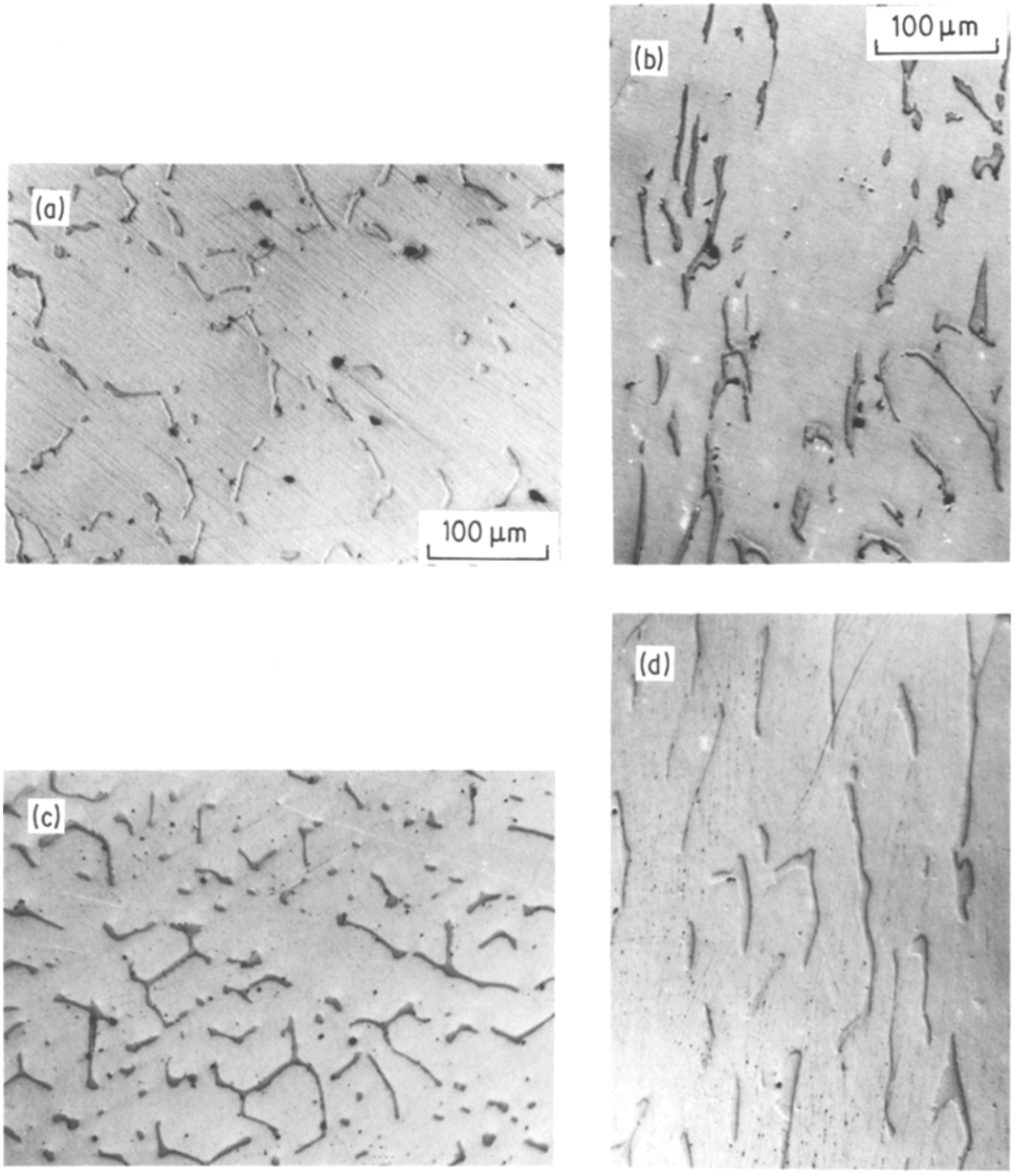

Figure 5 Metallurgical micrographs of transverse (a and c) and longitudinal (b and d) sections of the ingots of the compositions deviated from the eutectic composition by 0.5 mol % toward each of the Bi_2O_3 (a and b) and $6Bi_2O_3 \cdot SiO_2$ (c and d), which were solidified at a rate of 0.5 mm h^{-1}.

crystals were 4.5 and 3.2 μm, respectively. The interfibre spacing was 10 μm for both compositions. At the lower part of the ingots, the structure was irregular: within a distance of 10 and 6 mm from the upper surface of the seed crystal layer, respectively, for the former and the latter compositions, irregular structure was obtained, in which either phase of the δ-Bi_2O_3 (Nb_2O_5) or the γ-$6Bi_2O_3 \cdot SiO_2$ was precipitated.

4. Discussion

As described above, the B–BS melts did not produce a well-aligned regular structure even at the eutectic composition and at the lowest solidification rate, whereas the BN–BS melts did so not only at the eutectic composition but also at the compositions which deviated greatly from that and even at higher solidification rates. This difference in the microstructure between the systems might be interpreted in terms of the slope of the liquidus line as follows.

According to Mollard and Flemings [8], the well-aligned regular structure is produced only when the solidification proceeds under plane-front conditions, that is, the solid–liquid interface advances maintaining a planar surface and two phases grow at the same rate. Such conditions are provided when the following requirement is fulfilled and no constitutional supercooling occurs in the melt ahead of the growing crystals.

$$G/R = -m(C_E - C_0)/D \quad (3)$$

where G is the temperature gradient at the solid–liquid interface, R the solidification rate, m the slope of the liquidus line on the phase diagram at the composition of the melt, C_E the eutectic composition, C_0 the composition of the melt, and D the effective diffusion coefficient of solute in the melt.

m is considerably larger in the system B–BS than in the system BN–BS. As seen from Figs. 2 and 3, the slope of the liquidus line is -45 and $+45°$ C/mol %, respectively, for both sides of the eutectic

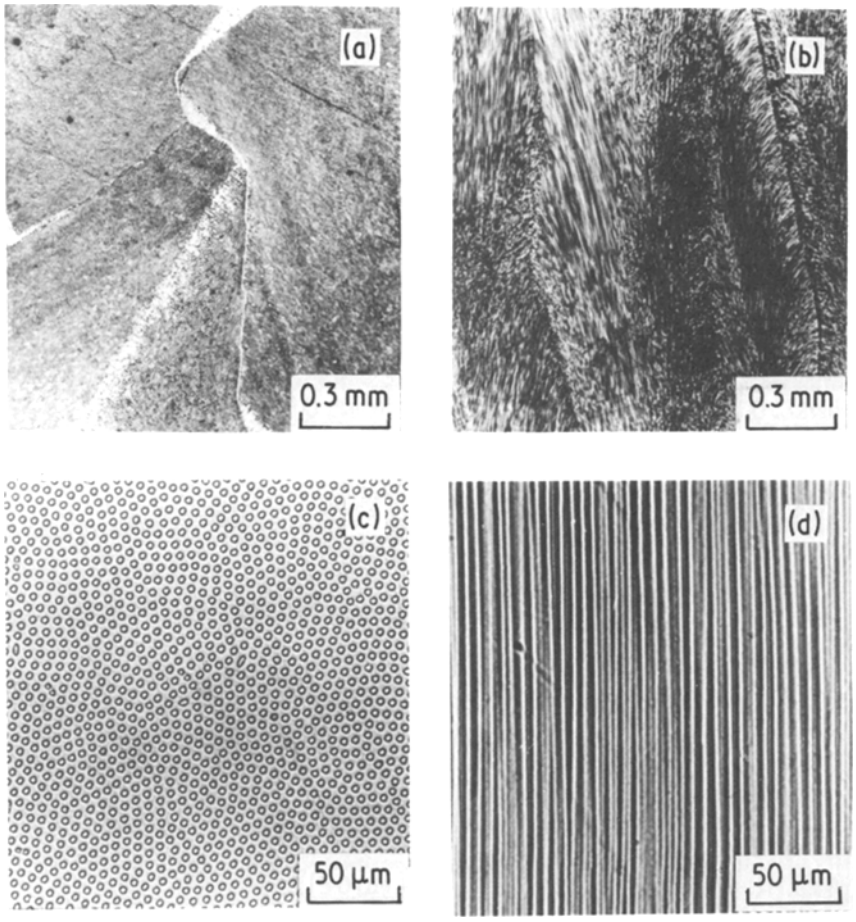

Figure 6 Polarizing micrographs of transverse (a and c) and longitudinal sections (b and d) of the ingot of the eutectic composition in the system BN–BS, which was solidified at a rate of 0.5 mm h^{-1}.

composition in the former system, whereas that is −2.8 and 2.3° C/mol %, respectively, in the latter system. D is considered not to differ so much between the two systems, but it may be only a little larger in the former due to a slightly simpler composition. Accordingly, the m/D ratio is considerably larger in the system B–BS than that in the system BN–BS.

This means that in the system B–BS, constitutional supercooling may tend to occur and the plane-front conditions are liable to be destroyed by a slight deviation of the composition from the eutectic composition, even at a high temperature gradient and a low solidification rate. In the system BN–BS, the constitutional supercooling may hardly occur, so that the plane-front conditions could be maintained even at compositions which deviated greatly from the eutectic composition and even at low temperature gradients and high solidification rates.

Fig. 9 shows optical micrographs of the longitudinal sections of the ingots of the eutectic compositions in the systems B–BS and BN–BS, which were solidified at a rate of 0.5 mm h^{-1}. The ingots were taken out of the furnace at the middle stage of the solidification and the remaining melt above the solidified ingot was removed by decantation. It can be confirmed from Fig. 9 that the solidification actually proceeds under the plane-front conditions in the BN–BS melt, but not in the B–BS melt. Accordingly, it can be concluded that the B–BS melts gave an irregular structure even at the eutectic composition and the lowest solidification rate, because of the large slope of the liquidus line, whereas the BN–BS melts gave a regular structure even at compositions which deviated greatly from the eutectic composition and the high solidification rates, because of the small slope of the liquidus line.

It has already been stated that the well-aligned regular structures obtained in the system BN–BS consisted of a number of regions with cystal alignment a little different from region to region. The cause of the occurrence of such regions might be attributed to the use of randomly-oriented polycrystals as seeds. It was previously shown by the present authors [5] that the γ-$6Bi_2O_3 \cdot SiO_2$ crystal grows as a number of columns with the crystallographic orientation very little different between them, when the $6Bi_2O_3 \cdot SiO_2$ melt is undirectionally solidified using polycrystals as seeds. If the matrix phase of γ-$6Bi_2O_3 \cdot SiO_2$ crystal grows similarly in the present system, naturally the fibrous δ-Bi_2O_3 (Nb_2O_5) crystals would take a specific crystallographic relationship to the matrix phase, showing different alignments depending on those of the γ-$6Bi_2O_3 \cdot SiO_2$ columns.

At compositions deviating from the eutectic composition in the system BN–BS by 10 mol %, a well-aligned regular structure was obtained only in the upper part of the ingot. This is because the steady-state conditions [8] for the co-precipitation of the two phases could be attained at a later stage of the solidification. At any early stage of the solidification, only either one of the two phases constituting the eutectic system precipitated.

The volume fractions of the fibrous crystals observed for the ingots giving the well-aligned regular structure were 0.17, 0.23 and 0.14 for the eutectic

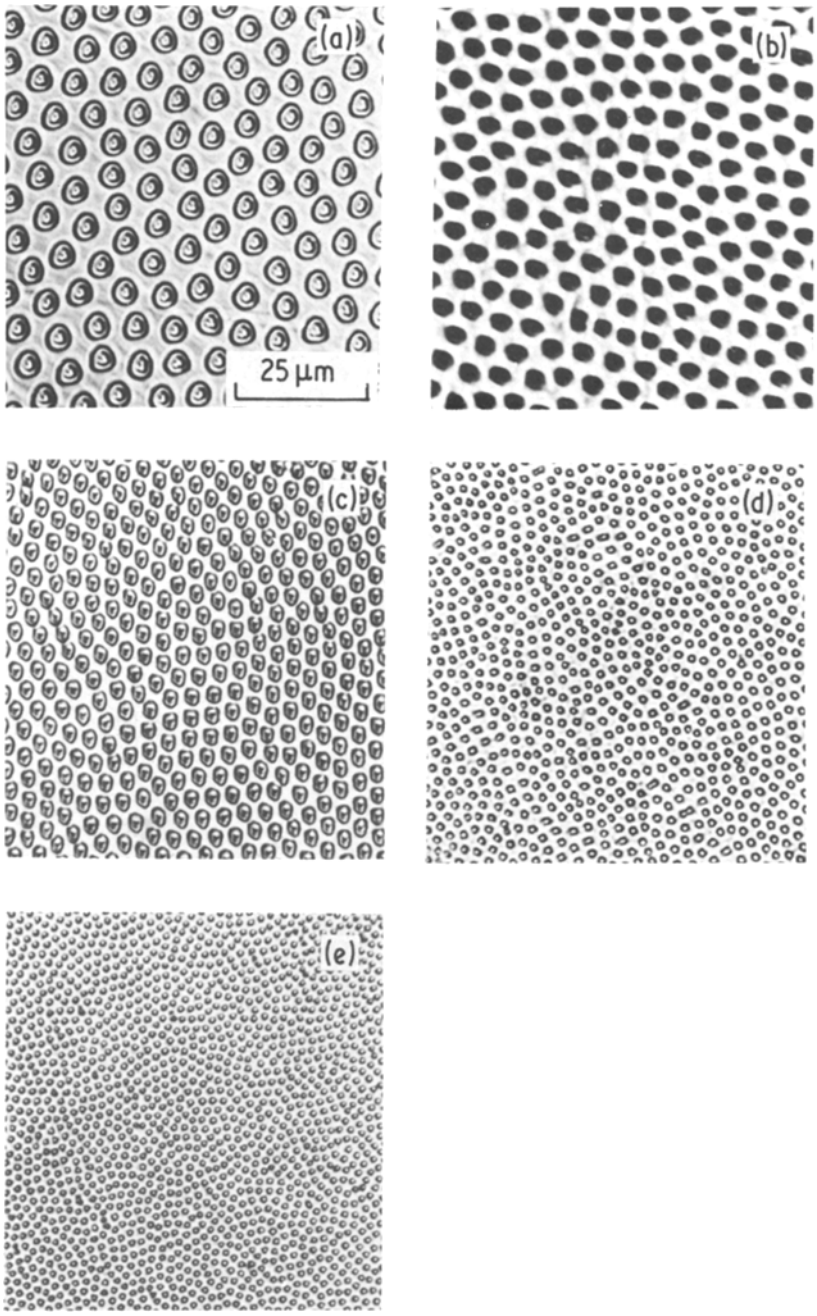

Figure 7 Polarizing micrographs of transverse sections of the ingots of the eutectic composition in the system BN–BS, which were solidified at a rate of (a) 0.5, (b) 1.0, (c) 2.5, (d) 5.0 and (e) 10 mm h^{-1}.

composition and the two compositions deviated from that to each side by 10 mol %, respectively, as already described. All three values almost coincide with those calculated from the respective starting compositions and the densities of the δ-Bi_2O_3 (Nb_2O_5) and γ-$6Bi_2O_3 \cdot SiO_2$ crystals measured by a pycnometer method. Considering that these volume fractions are all less than 0.28, it is reasonable that the minor δ-Bi_2O_3 (Nb_2O_5) phase took the fibrous form but not the lamella form. It is known [9] that at the volume fraction of the minor phase less than 0.28, the surface area of the interface between the two phases constitut-

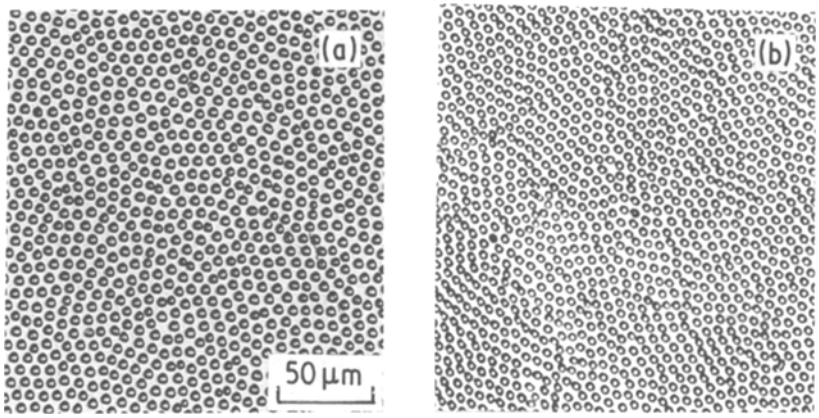

Figure 8 Polarizing micrographs of transverse sections of the ingots of the composition deviated from the eutectic composition by 10 mol % toward the Bi_2O_3 (Nb_2O_5) (a) or $6Bi_2O_3 \cdot SiO_2$ (b). They were cut at the distance of 12 mm from the upper surface of the seed crystal layer. The solidification rate was 0.5 mm h^{-1}.

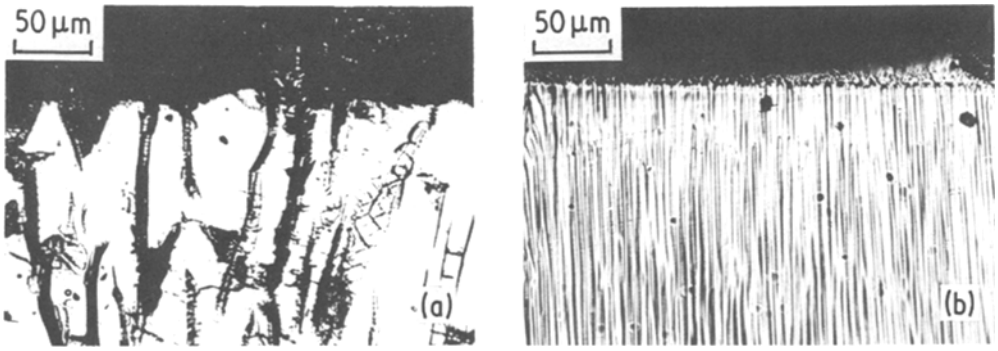

Figure 9 Front of the crystals growing from the eutectic melts in the system (a) B–BS and (b) BN–BS on the unidirectional solidification at a rate of 0.5 mm h^{-1}.

ing the eutectic system will become smaller, and accordingly the total interface energy will be less when the minor phase takes the fibrous form. It is interesting that the composition of the melt causes a considerable change of the volume fraction of the fibrous crystals without giving an essential change of the structure of the solidified ingot: the volume change was accomplished by the change of the diameter of the fibrous crystals with interfibre spacing being kept constant, as described in Section 3.2.2.

The diameter of the fibrous crystals, d, and the interfibre spacing, λ, of the eutectic ingots in the system BN–BS are plotted against reciprocal of square root of solidification rate, $R^{1/2}$, in Fig. 10. It can be seen from Fig. 10 that d and λ are related linearly to $R^{-1/2}$, and expressed by

$$d = 2.5\, R^{-1/2} \quad (4)$$

$$\lambda = 6.9\, R^{-1/2} \quad (5)$$

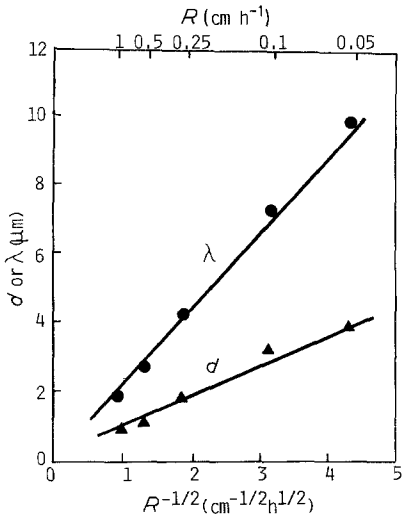

Figure 10 Fibre diameter, d, and interfibre spacing, λ, plotted against square root of solidification rate (R) for ingots of the eutectic composition in the system BN–BS.

Similar relations have been reported for many metal and oxide eutectics [9].

The δ-Bi_2O_3 (Nb_2O_5) crystal has a higher refractive index than the γ-$6Bi_2O_3 \cdot SiO_2$ crystal. Accordingly, the transverse thin section of the BN–BS ingots with the well-aligned structure may act as an image transmitter like a bundle of optical fibres [10], and might be usefully applied as a screen of a cathode ray tube and similar devices.

Acknowledgements

The authors thank Professor S. Sakka, Institute for Chemical Research, Kyoto University, for helpful suggestions. This research was supported by Grant in Aid for Special Research, Studies of Functional Ceramics (No. 58208021) of Ministry of Education, Science and Culture, Japan.

References

1. S. G. LIPSON and P. NISENSON, *Appl. Optics* **13** (1974) 2052.
2. M. PELTIER and F. MICHERON, *J. Appl. Phys.* **48** (1977) 3683.
3. R. E. ALDRICH, S. L. HOU and M. L. HARVILL, *ibid.* **42** (1971) 493.
4. J. P. HUIGNARD and J. P. HERRIAN, *Appl. Optics* **16** (1977) 1807.
5. HO-KUN KIM, S. ITO, T. KOKUBO and M. TASHIRO, *Yogyo-Kyokai-Shi* **89** (1981) 323.
6. HO-KUN KIM, T. KOKUBO, S. ITO and M. TASHIRO, *ibid.* **90** (1982) 348.
7. E. M. LEVIN and R. S. ROTH, *J. Res. Nat. Bur. Stand.* **68A** (1964) 197.
8. F. R. MOLLARD and M. C. FLEMINGS, *Trans AIME* **239** (1967) 1526.
9. W. J. MINFORD, R. C. BRADT and V. S. STUBICAN, *J. Amer. Ceram. Soc.* **62** (1979) 154.
10. J. D. PARSONS and A. S. YUE, US Patent 4 252 408 (1981).

Received 20 May
and accepted 18 June 1985